Morphology and developmental traits of the trilobite *Changaspis elongata* from the Cambrian Series 2 of Guizhou, South China

GUANG-YING DU, JIN PENG, DE-ZHI WANG, QIU-JUN WANG, YI-FAN WANG, and HUI ZHANG

Du, G.-Y., Peng, J., Wang, D.-Z., Wang, Q.-J., Wang, Y.-F., and Zhang, H. 2019. Morphology and developmental traits of the trilobite *Changaspis elongata* from the Cambrian Series 2 of Guizhou, South China. *Acta Palaeontologica Polonica* 64 (4): 797–813.

The morphology and ontogeny of the trilobite *Changaspis elongata* based on 216 specimens collected from the Lazizhai section of the Balang Formation (Stage 4, Series 2 of the Cambrian) in Guizhou Province, South China are described. The relatively continuous ontogenetic series reveals morphological changes, and shows that the species has seventeen thoracic segments in the holaspid period, instead of the sixteen as previously suggested. The development of the pygidial segments shows that their number gradually decreases during ontogeny. A new dataset of well-preserved specimens offers a unique opportunity to investigate developmental traits after segment addition is completed. The ontogenetic size progressions for the lengths of cephalon and trunk show overall compliance with Dyar's rule. As a result of different average growth rates for the lengths of cephalon, trunk and pygidium, the length of the thorax relative to the body shows a gradually increasing trend; however, the cephalon and pygidium follow the opposite trend. Morphometric analysis across fourteen post-embryonic stages reveals growth gradients with increasing values for each thoracic segment from anterior to posterior. The reconstruction of the development traits shows visualization of the changes in relative growth and segmentation for the different body parts. The new dataset and growth gradient of the trunk suggest that the thoracic segment growth dynamics of early Cambrian to Silurian trilobites follow the same general continuous, steady-state growth gradient decreasing from posterior to anterior.

Key words: Trilobita, Oryctocephalinae, *Changaspis*, developmental traits, ontogeny, Cambrian, China.

Guang-Ying Du [544840279@qq.com], College of Resource and Environment Engineering, Guizhou University, 2708 South Section of Huaxi Avenue., Guiyang, 550025, China; and College of Information Engineering, Guizhou University of Traditional Chinese Medicine, Dongqing South Road, Guiyang, 550025, China.
Jin Peng [gzpengjin@126.com] (corresponding author), De-Zhi Wang [1440823413@qq.com], Qiu-Jun Wang [18785177085@qq.com], Yi Fan Wang [256797947@qq.com], and Hui Zhang [724291335@qq.com], College of Resource and Environment Engineering, Guizhou University, 2708 South Section of Huaxi Avenue, Guiyang, 550025, China.

Received 1 February 2019, accepted 22 July 2019, available online 13 November 2019.

Introduction

The ontogeny of corynexochide trilobites has rarely been studied. McNamara et al. (2003, 2006) described the ontogeny of four oryctocephalid genera, *Arthricocephalus* Bergeron, 1899; *Balangia* Chien, 1961; *Changaspis* Lee in Chien, 1961 and *Duyunaspis* Chang and Chien in Zhou et al., 1977. Recently, Dai et al. (2014, 2017) reported the ontogeny of the cheiruroidid trilobite *Hunanocephalus* Lee in Lu et al., 1963 and the oryctocephalid *Duyunaspis* Chang and Chien in Zhou et al., 1977. Hou et al. (2015) reported the ontogeny of the oryctocephalid *Duodingia* Chow in Lu et al., 1974. Lei (2015) reported the ontogeny of the oryctocephalid *Duyunaspis* Chang and Chien in Zhou et al., 1977. More recently, Esteve et al. (2017) described the ontogeny of the oryctocephalid *Oryctocephalus indicus* Reed, 1910.

Changaspis elongata Lee in Chien, 1961, is the type species of the genus and was first described on the basis of material from the Cambrian Series 2 of the Balang Formation near Duyun City, eastern Guizhou Province, China (for synonymy, see McNamara et al. 2006; Qin et al. 2010). It is charac-

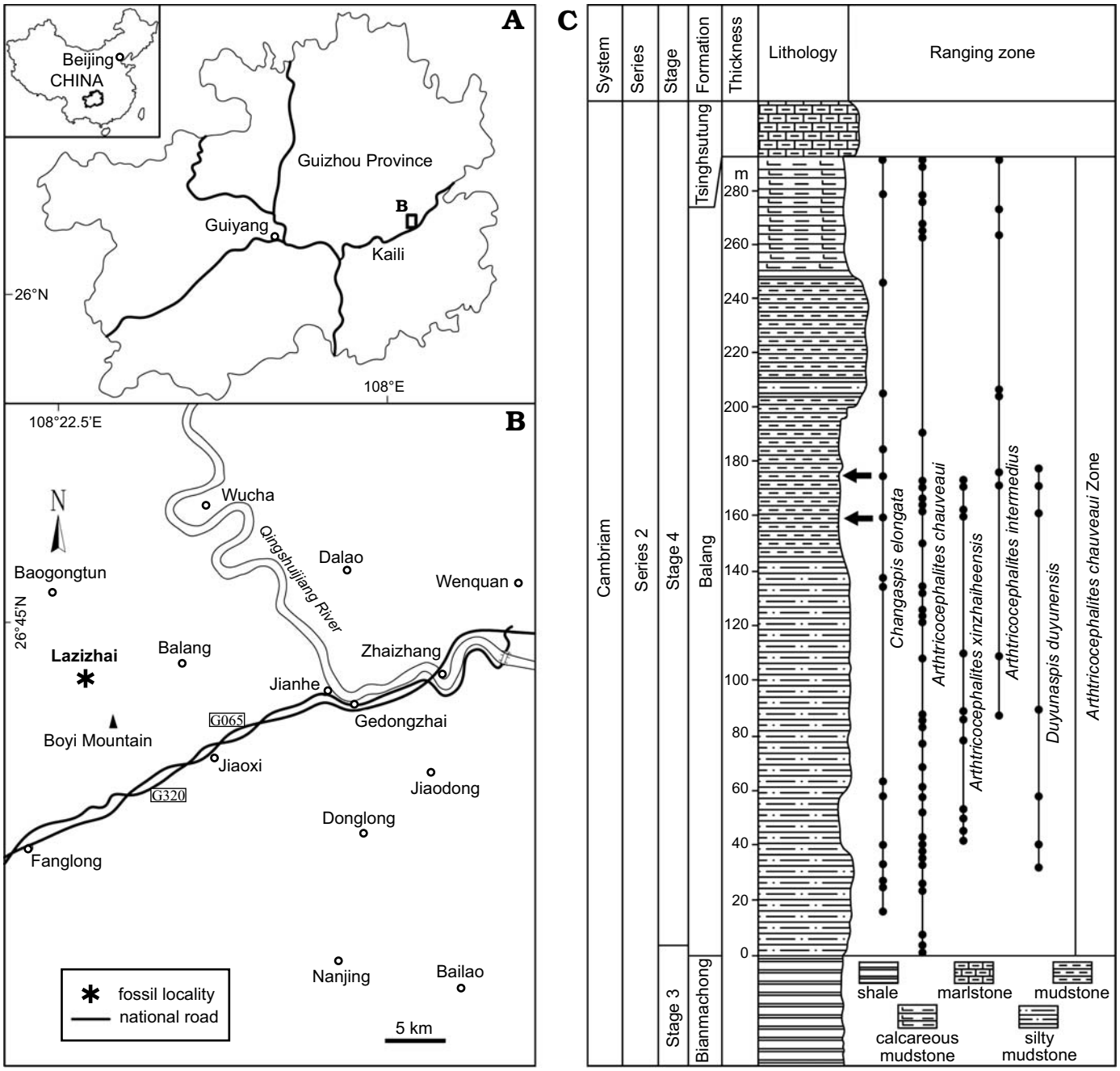

Fig. 1. **A**. Map showing the position of collecting localities in the Guizhou Province. **B**. Map of the fossil locality Lazizhai, 6.4 km from Jianhe, Guizhou Province, South China. **C**. Stratigraphical column of the Balang Formation (Cambrian Stage 4), showing the horizon where the material was collected (arrows), and the stratigraphic occurrences of oryctocephalid trilobites.

terized by having a large glabella expanding anteriorly, four pairs of glabellar furrows, long pleural spines, fourteen to fifteen thoracic segments and a very small pygidium (Chien 1961). Subsequently, some materials of this species were described and illustrated by McNamara et al. (2006) and Qin et al. (2010), who suggested that the pygidium maintained a solitary terminal axial piece during ontogeny and that the holaspides had sixteen thoracic segments. However, the specimens in this study show some differences from those described previously. The most notable difference is that eight complete specimens have seventeen thoracic segments, rather than sixteen in the holaspides. In addition, the well-preserved ontogenetic specimens show that there are multiple segments of the pygidium from meraspid degrees 4 to 16. This observation means that the material of the ontogenetic sequence formerly illustrated consisted solely of the meraspides, and the number of the pygidial segments was variable during ontogeny. Therefore, its ontogenetic sequence needs to be reinvestigated in order to reveal new details of morphological changes from the meraspid degree 4 to the holaspid period.

The description of ontogenetic changes has become a standard part of palaeontological analysis, and increasingly

more quantitative methods are used to describe and differentiate development modes (Hughes et al. 2017). Recently, quantitative studies of the developmental traits of Silurian trilobite *Aulacopleura koninckii* Barrande, 1852. have received attention because this fossil may provide insight into how segment growth dynamics changed during post-embryonic development and how evolutionary development biology is correlated with fossils (e.g., Fusco et al. 2004, 2012, 2014, 2016; Hughes et al. 2017). The extraordinary abundance of well-preserved exoskeletons of *Changaspis elongata* provides a unique opportunity to quantitatively explore the developmental traits, including the variations in the relative axial length of different body and trunk parts, the growth gradients of the relative axial growth rates and absolute axial growth rates, the growth progression, and the average growth rates for the lengths of body, cephalon, trunk, and pygidium. Here, we document a partial ontogenetic sequence of *C. elongata* based on a large number of well-preserved specimens from the Balang Formation, Guizhou Province, China. We also exploit the dataset of well-preserved specimens of *C. elongata*, which contains accurate measurements of the axial lengths of body, cephalon, trunk, pygidium and individual thoracic segments from the meraspid degree 4 to the holaspid period. These developmental traits are based on thirteen developmental stages of the meraspid degree and one holaspid stage from the meraspid degree 4 (four TSs) to the holaspid period (with 17 TSs). In this paper, the quantitative research methods previously applied to *A. koninckii* (Hughes et al. 2017) are used to calculate the developmental traits of *C. elongata*.

Institutional abbreviations.—GZRCP GU, Guizhou Research Centre for Paleontology of Guizhou University, Guiyang, China; JLZ, specimens are collected from Lazizhai section at Jianhe County,Guizhou Province, China.

Other abbreviations.—AGI, per-moult growth increment; AGR, average per-moult growth rate; BOL, body length; CEL, cephalic length; D4–16, meraspid degrees 4–16; H, holaspid period; IDC, index of conformity to Dyer's rule; JLZ-n, n meters above the base of Lazizhai section; L1–A, glabellar lobes; LTS, length of thoracic segment; S0–4, glabellar furrows; TS, thoracic segment; TRL, trunk length.

Material and methods

The Cambrian Balang Formation contains an ample fauna of trilobites, including *Probowmania* (*Probowmania*) *balangensis* Yuan and Zhao in Yuan et al., 1997, *Redlichia* (*Pteroredlichia*) *chinensis* Walcott, 1905, *Arthricocephalus chauveaui* Bergeron, 1899, and *Arthricocephalites xinzhaiheensis* Chien and Lin in Lu et al., 1974, *Arthricocephalites intermedius* Zhou in Lu et al., 1974, *Changaspis elongata* Lee in Chien, 1961, *Duyunnaspis duyunensis* Chang and Chien in Zhou et al., 1977, and *Balangia balangensis* Chien, 1961 (Peng et al. 2005, 2006; Qin et al. 2010; Shen et al. 2016; Liang et al. 2017; Du et al. 2018). Approximately 211 complete specimens studied herein were collected from the mudstone of the Balang Formation (Stage 4, Series 2 of the Cambrian) at the Lazizhai section, approximately 6.4 km northwest of Jianhe County, Guizhou Province, South China (Fig. 1). To eliminate the influence of shearing and longitudinal or transversal elongation as far as possible, the well-preserved complete exoskeletons of 147 intact specimens from two horizons, 160 m and 175 m of the Lazizhai section, were selected for the quantitative studies, i.e., linear measurements of the exoskeleton (Fig. 1); these specimens belong to developmental stages from the meraspid to holaspid, including 2 D4, 3 D5, 3 D6, 3 D7, 5 D8, 6 D9, 9 D10, 12 D11, 25 D12, 24 D13, 30 D14, 8 D15, 9 D16, and 8 H.

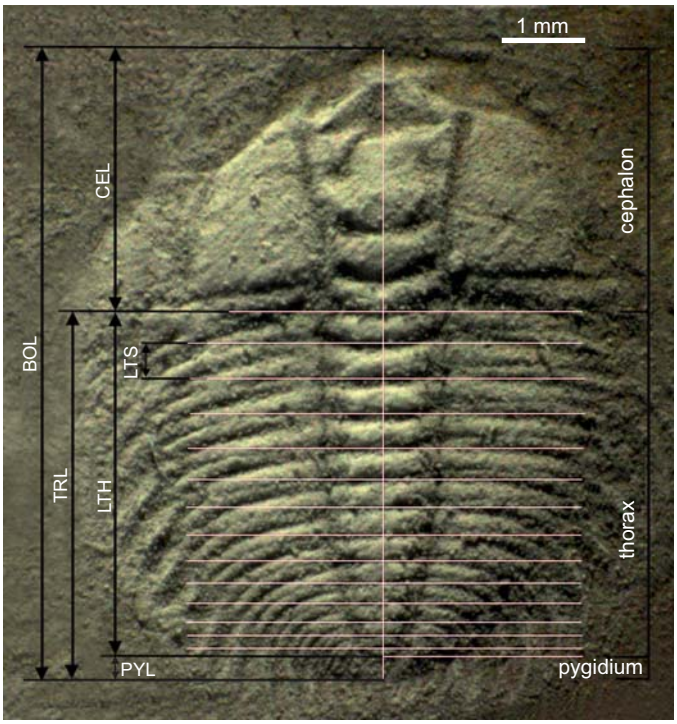

Fig. 2. Major anterior-posterior body divisions measured on oryctocephalid trilobite *Changaspis elongata* Lee in Chien, 1961 (D14 with 14 thoracic segments, JLZ-160-1006). A line along the sagittal axis was constructed on the image of each specimen and for each segment a line was then placed transversely to this, linking the articulating processes at the fulcral boss (the point abaxially marginal to the fulcrum). The intersections of these lines with the sagittal axis were used to calculate the length of each thoracic segment i (LTS_i). LTS_2 is shown as an example. Thorax plus pygidium together constitute the trunk. Cephalon, thorax and pygidium make up the body. BOL, body length; TRL, trunk length; CEL, cephalic length; LTH, length of thorax; PYL, pygidial length; LTS_i, length of each thoracic segment i.

To obtain the data about the length of the exoskeleton, we construct a line along the sagittal axis on the image of each sample with the AutoCAD software. Then, a transverse line is placed crosswise to connect the fulcrum bump (the point on the back edge of the fulcrum) for each thoracic segment. The intersection of the line and the sagittal axis is used to represent axial rings of each thoracic segment, and

the lengths of cephalon, thorax and pygidium are recorded (Fig. 2). The linear distance between two intersecting lines of transverse and longitudinal axes is calibrated with the ruler. The growth dataset of average measures at each developmental stage is used to explore the developmental traits for the lengths of the cephalon, thorax, thoracic segments, pygidium, trunk, and body from meraspid degree 4 to the holaspid period. For measurement data of different body parts, see SOM: table S1, Supplementary Online Material available at http://app.pan.pl/SOM/app64-Du_etal_SOM.pdf.

The constant rate of per-moult size increase is known as the so-called Dyar's rule (Dyar 1890). The index of conformity to Dyar's rule (IDC) is a continuous metric that quantifies the fit of the growth progression at a constant rate during ontogeny, and the "coarse-grained" quantitative approach is used to evaluate the conformity to Dyar's rule (Fusco et al. 2012). Therefore, the values of conformity to Dyar's rule for the lengths of cephalon and trunk are calculated according to the formula derived by Fusco et al. (2012). For the specific calculation formula and formula parameters, see the article by Fusco et al. (2012), and for details on the estimation of IDC values for the lengths of cephalon and trunk from the D4–16 are given in the SOM: table S2.

The average per-moult growth rates (AGR) of the lengths of the body (BOL), cephalic length (CEL) and trunk length (TRL) from D4–16 are calculated as the inverse logarithm of the average per-moult growth increment (AGI), and the natural logarithmic transformation of the original variables at each ontogenetic stage is carried out (Fusco et al. 2014). AGI values are calculated as the arithmetic mean of ln(BOL), ln(CEL), and ln(TRL) increments between adjacent pairs of two stages in the ontogenetic sequence (Fusco et al. 2012). For details on the estimation of AGR values and standard errors for BOL, CEL, and TRL, see SOM: table S2. The AGR of the length of individual thoracic segments are calculated in the same way. For details of the estimation of the AGR values and standard errors caused by structural deformation and measurement, see SOM: table S3.

The ontogenetic allometric coefficients of the length of each thoracic segment (LTS) with respect to trunk length (TRL) represent relative axial growth rates. Therefore, the relative axial growth rates of each segment (i segment) at each development stage (d stage) are calculated as the linear regression slope of $\ln(LTS_{i,d})$ versus $\ln(TRL_d)$ (Fusco et al. 2014) (n = 14 for TS1–4, n decreases from n = 13 for TS5 to n = 2 for TS16). For the values of $\ln(LTS_{i,d})$ and $\ln(TRL_d)$, we use the mean values rather than the sample measurement dataset. For details on the estimation of the allometric coefficients and standard errors resulted from structural deformation and measurement of each thoracic segment, see SOM: table S3.

Results

Description of ontogeny

The ontogenetic series of *Changaspis elongata* described herein ranges from meraspid degree 4 to the holaspid period (Figs. 3–6). The ontogenetic tracing of each meraspid degree is mainly based on the number of thoracic segments. During the holaspid period, the number of thoracic segments remains fixed regardless of size. The number of specimens and thoracic segments and the lengths of the exoskeletons at each ontogenetic stage are provided in Table 1. Because the thoracic–pygidial boundary is difficult to recognize in some oryctocephalid trilobites with pleural spines in the thorax (Esteve et al. 2017), the posterior part of the trunk is carefully observed in detail. Morphological changes during ontogeny are shown in Fig. 7. The main morphological variations are as follows:

Meraspid degree 4.—Two complete exoskeletons, of which one specimen is figured (Fig. $3A_1$). Cranidium semi-circular in outline, obviously convex. Cranidial length approximately half as long as body. Anterior margin curved anteriorly; anterior border wide and of uniform width. Glabella wide and parallel-sided from L1 to L3 and then slightly expanded anteriorly from L4 to LA, reaching the anterior border furrow. Glabellar furrows weakly impressed, S1–4 indistinct; axial furrow of glabella weakly impressed. Eye ridge weakly defined, located anteriorly, close to anterior border. Palpebral lobe and facial suture indistinct. Fixigena broad; librigena extraordinary narrow. Genal spine indistinct. Posterior margin bent laterally. Posterior border narrow and shallow; posterior border furrow shallow, extending anterolaterally.

Table 1. Number of specimens (N) and length range of exoskeleton of *Changaspis elongata* at each ontogenetic stage.

Ontogenetic stages	N	Length range (in mm)
Meraspid degree 4	2	1.44–1.46
Meraspid degree 5	4	2.04–2.09
Meraspid degree 6	6	2.21–2.25
Meraspid degree 7	5	2.23–2.70
Meraspid degree 8	14	2.48–3.00
Meraspid degree 9	16	2.67–4.27
Meraspid degree 10	22	3.45–6.05
Meraspid degree 11	19	3.76–5.15
Meraspid degree 12	26	3.17–9.58
Meraspid degree 13	28	4.40–9.94
Meraspid degree 14	30	5.54–15.53
Meraspid degree 15	20	5.41–17.40
Meraspid degree 16	11	6.88–17.12
Holaspid stage	8	17.73–21.10

Fig. 3. Meraspid exoskeletons of oryctocephalid trilobite *Changaspis elongata* Lee in Chien, 1961 from the Balang Formation (Cambrian Stage 4), Jianhe County, Guizhou Province, South China. **A**. D4, JLZ-175-161; close-up of the 4 thoracic segments and pygidium (A_2). **B**. D5, JLZ-160-42; close-up of the last 3 thoracic segments and pygidium (B_2). **C**. D6, JLZ-160-555; close-up of the last 4 thoracic segments and pygidium (C_2). **D**. D7, JLZ-160-1359; close-up of the last 4 thoracic segments and pygidium (D_2). The arrows represent the position of the thoracic-pygidial boundary. Scale bars 0.5 mm. →

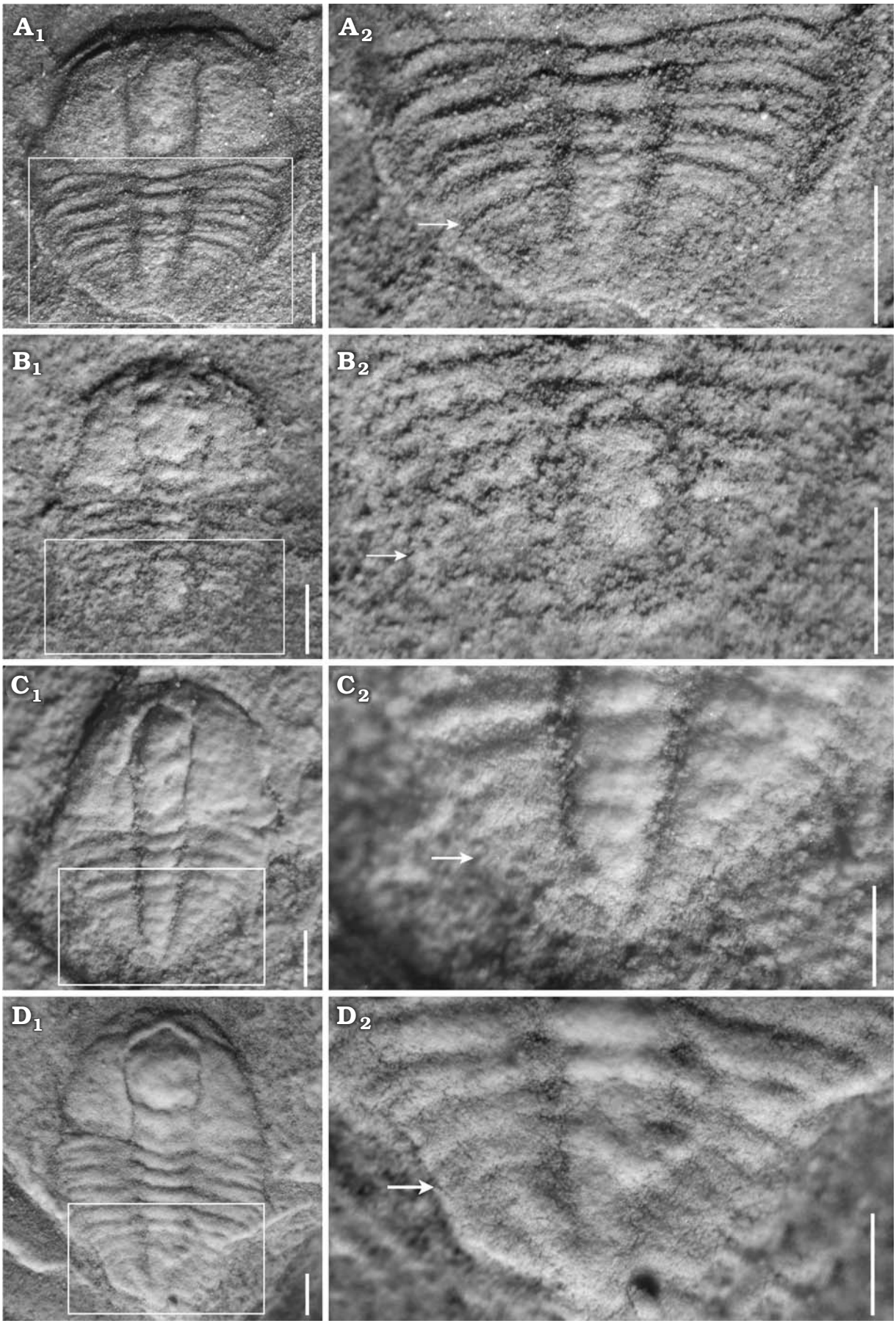
A1
A2
B1
B2
C1
C2
D1
D2

Thorax with four segments. Axial ring distinctly developed, defined by deep axial furrows, slightly less than half the pleural width. Pleurae slightly curved backward, with four tapered pleural tips. Pleural furrow deeply concave and extends laterally further. Pleural spine indistinct.

Pygidium semi-circular in outline. Axis narrow, tapering backward, with posterior tip close to posterior border. Pleural field slightly convex, interpleural furrows and pleural furrow faint. Axial rings faint, and four axial rings faintly visible (Fig. $3A_2$).

Meraspid degree 5.—Four complete exoskeletons, of which one specimen is figured (Fig. $3B_1$). Cranidium semi-elliptical in outline, moderately convex. Glabellar furrows distinctly impressed; four pairs of glabellar furrows connecting to axial furrows: S1 linked by weak transglabellar furrow in the middle, S2–4 pit-like. Palpebral lobe crescentic, curved outward. Anterior branch of facial suture slightly convergent forward, posterior branch extending to lateral border. Facial suture proparian slightly impressed. Occipital ring moderately convex. Fixigena wide and protuberant. Thorax with five segments. Pleural lobe defined by four pairs of shallow interpleural furrows. Pygidium small, tapered in outline, with posterior margin not preserved. Pleural furrow and interpleural furrow faint. Three axial rings of pygidium faintly visible (Fig. $3B_2$).

Meraspid degree 6.—Six complete exoskeletons, of which one specimen is figured (Fig. $3C_1$). Cranidial length approximately two-thirds as long as body. Glabella wider than that of degree 5, slightly expanded anteriorly from L1 to L4, with anterior margin reaching anterior border furrow; four pairs of glabellar furrows obviously impressed; S1 transverse and deep; S2–4 pit-like and not extending to axial furrows. Posterior branch of facial suture extended to genal angle. Facial suture gonatoparian and moderately impressed. Eye ridge moderately defined; palpebral lobe crescentic, curved outward. Fixigena broad and moderately convex. Thorax with six segments. Axis moderately convex, defined by shallow axial furrows. Pygidium wider than in previous stage. Axial ring poorly defined, and two axial rings faintly visible (Fig. $3C_2$).

Meraspid degrees 7–10.—Fifty-seven complete exoskeletons, of which four specimens are figured (Figs. 3D, $4A_1$, B_1, C_1). Generally, exoskeletons range from 2.23 mm to 6.05 mm in length. In addition to extra thoracic segments, major changes in these degrees are subtle. They are shown by the proparian suture in degree 7 (Fig. $3D_1$), with a gradual shift of posterior branches towards the genal angle and by gonatoparian sutures in degrees 8, 9, and 10 (Fig. $4A_1$, B_1, C_1); narrow palpebral lobes in meraspid degrees 7 and 8 (Figs. $3D_1$, $4A_1$) to moderately wide in degrees 9 and 10 (Fig. $4B_1$, C_1); poorly defined eye ridges in degrees 7 and 8 (Figs. $3D_1$, $4A_1$) that become distinct in degrees 9 and 10 (Fig. $4B_1$, C_1); absent genal spines in degrees 7 and 8 (Figs. $3D_1$, $4A_1$) that become short and defined in degrees 9 and 10 (Fig. $4B_1$, C_1). Axial rings faint, two axial rings faintly visible (Figs. $3D_2$, $4A_2$, B_2, C_1).

Meraspid degree 11.—Nineteen complete exoskeletons, of which one specimen is figured (Fig. $4D_1$). Glabella wider than that of degree 10, parallel-sided from L1 to L2 and then obviously expanded anteriorly from L3 to LA, with anterior margin reaching anterior border furrow. Glabellar furrows evidently impressed, extending to axial furrows. Anterior border broad and flat posterior border slightly prominent and extending backward into short genal spine.

Thorax with eleven segments. Axial rings become wider proportionally than for the previous degree. Ratio of width of axial lobe to pleural lobe greater. Interpleural furrow deeper than that of degree 10. Articulated half rings distinct. Pleural spines well defined, extending strongly backward. Pleural lobes slightly longer than pleural spines. Pygidium relatively even smaller than that of meraspid degree 10 (Fig. $4D_2$).

Meraspid degree 12.—Twenty-six complete exoskeletons, of which one specimen is figured (Fig. $5A_1$). This degree is similar to D11, but it has a more distinct eye ridge and deeper axial furrows; relatively deeper posterior border; wider fixigena. Pygidium relatively even smaller than that of previous degree (Fig. $5A_2$).

Meraspid degree 13.—Twenty-eight complete exoskeletons, of which one specimen is figured (Fig. $5B_1$). Exoskeleton becomes wider with smaller length/width ratio than that of D12. With the gradual shift of posterior branches towards the posterior border, facial sutures become opisthoparian. Axial rings of thorax wider proportionally than those of previous degree. Thirteen pleurae equal in width to width of pleural spines of thorax. Pygidium relatively even smaller than that of D12; a pair of short pygidial spine is present in the terminal axial piece (Fig. $5B_2$).

Meraspid degrees 14–16.—Sixty-one complete exoskeletons, of which three specimens are figured (Figs. $5C_1$, D_1, $6A_1$). Generally, exoskeletons range from 5.54 mm to 17.12 mm in length. In addition to extra thoracic segments, major changes in these degrees are not obvious.

These stages are mainly characterized by short genal spines; wide palpebral lobe; well-defined eye ridge in degree 14 (Fig. $5C_1$) that becomes progressively larger in D15 and D16 (Figs. $5D_1$, $6A_1$); large pleural spines in the thorax and short pygidial spine in D14, 15 (Fig. $5C_1$, D_1) that become progressively larger reaching the holaspid size in D16

Fig. 4. Meraspid exoskeletons of oryctocephalid trilobite *Changaspis elongata* Lee in Chien, 1961 from the Balang Formation (Cambrian Stage 4), Jianhe County, Guizhou Province, South China. **A**. D8, JLZ-160-1013; close-up of the last 6 thoracic segments and pygidium in (A_2). **B**. D9, JLZ-175-103; close-up of the last 5 thoracic segments and pygidium (B_2). **C**. D10, JLZ-175-1977; close-up of the last 3 thoracic segments and pygidium (C_2). **D**. D11, JLZ-160-753; close-up of the last 6 thoracic segments and pygidium (D_2). The arrows represent the position of the thoracic-pygidial boundary. Scale bars: A–C, 0.5 mm; D, 1 mm. →

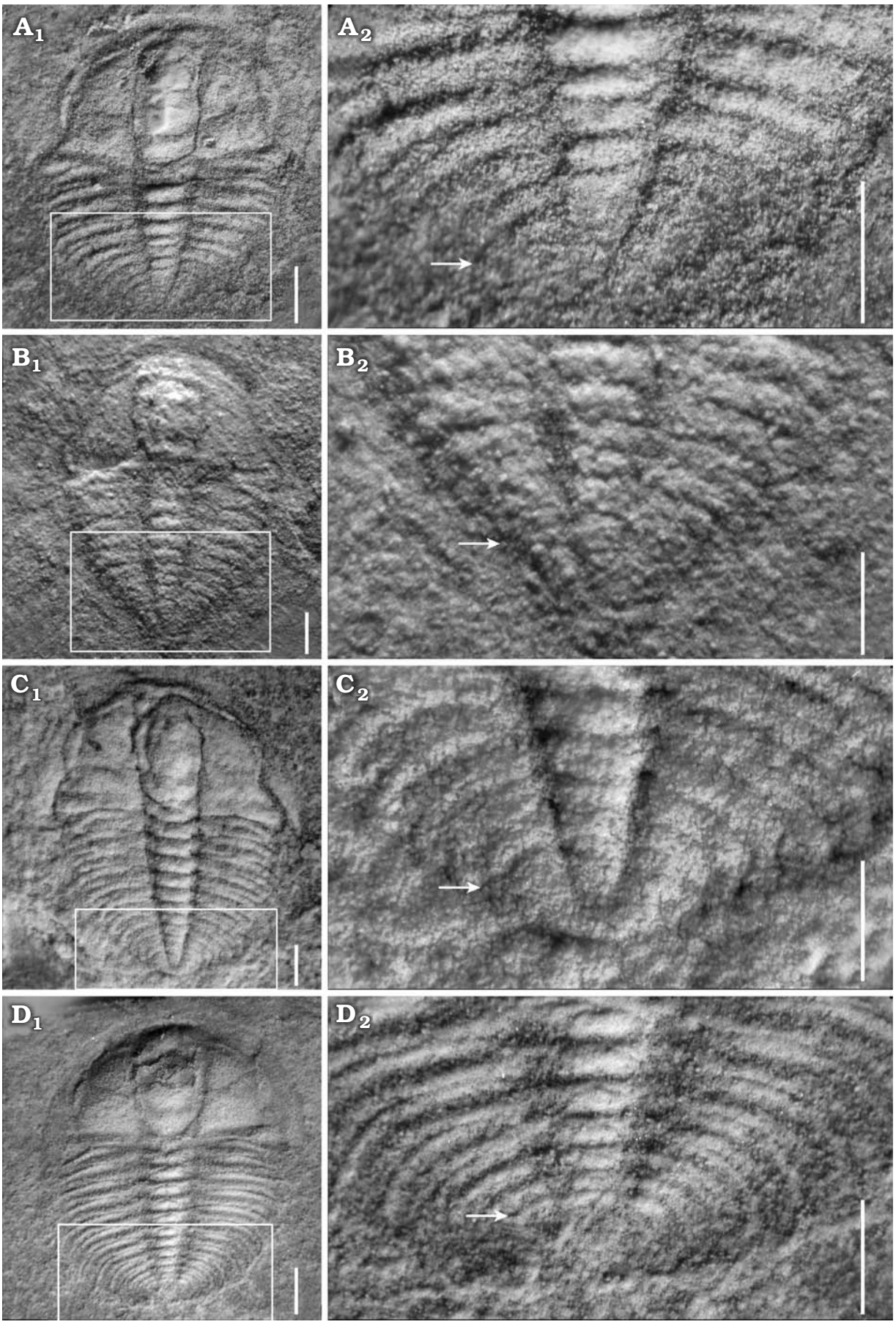
A1
A2
B1
B2
C1
C2
D1
D2

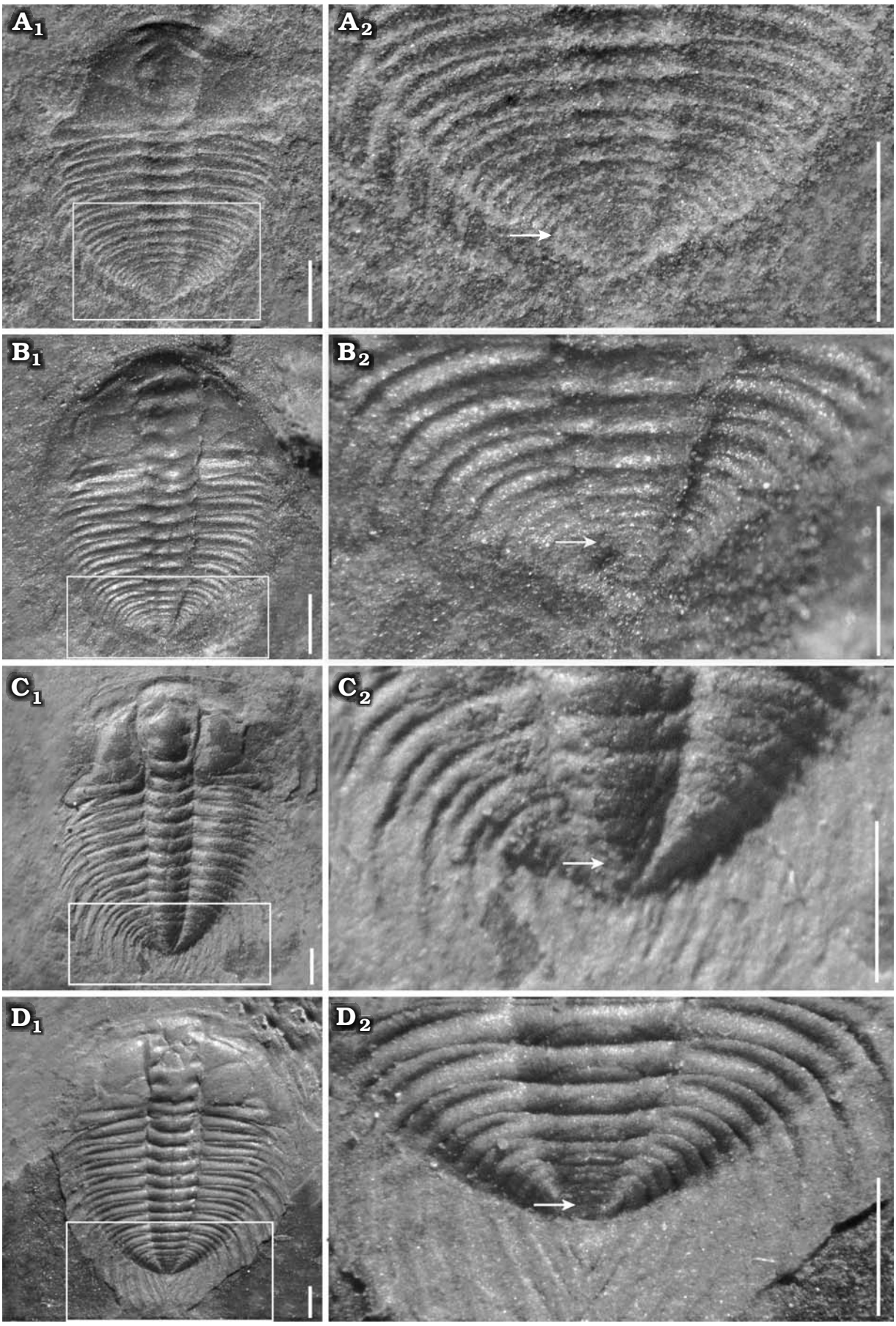
A1
A2
B1
B2
C1
C2
D1
D2

(Fig. $6A_1$). Axial rings faint and comprise two axial rings faintly visible in D15 and one axial ring faintly visible in D16.

Holaspid period.—Eight complete exoskeletons, of which three specimens are figured (Fig. $6B_1$, C_1, D_1). Exoskeleton elliptical in outline; cephalon semi-elliptical in outline, the transverse width of cranidium greater than its longitudinal length. Glabella of moderate convexity, expanded anteriorly, the maximum width opposite L4; frontal glabellar lobe clearly expanded anteriorly, with anterior margin across anterior border furrow and reaching anterior border. Four pair of glabellar furrows evidently impressed, S2–4 pit-like, obviously not extending to axial furrows, S1 connected across middle of glabella. Eye ridge and palpebral lobe clearly prominent; palpebral lobe long, slightly curved and extending posteriorly close to the posterior border furrow. Anterior branches short, slightly divergent forward, cutting anterior border in a rounded curve. Posterior branches extending to posterior border close to genal spine at about 40° from posterior end of palpebral lobe. Fixigena flat and broad. Librigena narrow and flat. Occipital furrow slightly curved rearwards. Anterior border broad with shallow anterior furrow. Posterior border of flat and uniform width, extending into short genal spine that bends back to the third thoracic segment.

Thorax with seventeen segments (Fig. $6B_2$, C_2, D_2). Axial width slightly less than that of pleural lobe. Axis convex, tapering rearwards. Articulating half rings well-defined. Pleural lobes extending slightly posteriorly, narrower than axis. Pleural furrows deep and bend backwards, extending to the end of pleural tip. Interpleural furrow shallow. Pleural spines long and flat. Pleurae slightly longer than pleural spine T1–6 and then slightly shorter T7–17.

Pygidium very small, sub-elliptical in outline, with posterior margin rounded, having only one terminal axial piece and extending posteriorly into a long, spindly pygidial spine (Fig. $6B_2$, C_2, D_2).

Trunk segmentation sequence

The appearance of the cephalic-trunk articulation marks the beginning of the meraspid stage. During the subsequent meraspid moulting process, new articulations form between the segments of the anterior trunk, resulting in a group of articulating trunk segments called the thorax in front of the pygidium (Fusco et al. 2004). The successive ontogenetic sequence of *Changaspis elongata* from meraspid degree 4 to the holaspid period enables us to analyse the trunk segmentation pattern with respect to the dorsal exoskeletons. By studying the pattern of trunk segmentation during ontogeny, its schedule (Fig. 8) illustrates the following features:

The number of axial rings of the pygidium is vaguely visible during ontogeny. In D4–6 the number of pygidial segments may gradually decrease from 4 to 2 segments. However, four pygidial segments are recognized in D6–16. During the holaspid period, the pygidium maintains one terminal axial piece. This phenomenon suggests that the number of pygidial segments is variable during ontogeny, rather than fixed one terminal axial piece being present, as previously suggested, in D5–16 (McNamara et al. 2006). Therefore, the D5 of McNamara et al. (2006: 5, text-fig. 1-1) is actually D3.

In D4–14 new thoracic segments appear at the rear of the thorax. However, the number of trunk segments remains constant in D15, 16, and H. Trilobite ontogeny can be subdivided into an anamorphic phase and a subsequent epimorphic phase (Hughes et al. 2006, 2017). Therefore, the ontogeny of *C. elongata* passes through the anamorphic phase in D4–14 and the epimorphic phase in D15, 16, and H.

The meraspid degree 15 has the same number of trunk segments as the holaspid period. Therefore, the onset of the epimorphic phase at D15 precedes the onset of the holaspid phase. During the holaspid period, the pygidium contains only one terminal axial piece, and the thorax remains unchanged for 17 segments. The developmental mode of this species is the hypoprotomeric mode (Hughes et al. 2006).

Developmental traits

The well-preserved intact specimens and the morphological dataset allow us to define six developmental traits after segment addition is completed, which include the variations in the relative axial lengths of different body and trunk parts, the growth gradients of the relative axial growth rates and absolute axial growth rates, the growth progression for the length of cephalon and trunk, and the average growth rate for the length of body, cephalon and trunk.

Variations in the relative axial length of different trunk parts.—The results of morphometric analysis allowed to visualize patterns of relative growth and segmentation after thoracic segment addition has been completed at each anamorphic degree. By visualizing the changes in the relative trunk length of each thoracic segment and pygidium, the main changes (Fig. 9A) and reasons include the following features:

From D4 to H the proportion of the first to the seventh thoracic segments relative to the trunk decreases significantly (Fig. 9A) because the allometric coefficients with respect to trunk length are greater than 1 (Table 2). This means that the growth rates of the thoracic segments are slower than that of the trunk.

From D8 to H the proportions of the 8th and 9th thoracic segments to the trunk remain basically unchanged (Fig. 9A) because the coefficient of allometric growth is close to 1

← Fig. 5. Meraspid exoskeletons of oryctocephalid trilobite *Changaspis elongata* Lee in Chien, 1961 from the Balang Formation (Cambrian Stage 4), Jianhe County, Guizhou Province, South China. **A**. D12, JLZ-175-1167; close-up of the last 8 thoracic segments and pygidium (A_2). **B**. D13, JLZ-160-2023; close-up of the last 6 thoracic segments and pygidium (B_2). **C**. D14, JLZ-160-753; close-up of the last 6 thoracic segments and pygidium (C_2). **D**. D15, JLZ-175-30; close-up of the last 7 thoracic segments and pygidium (D_2). The arrows represent the position of the thoracic-pygidial boundary. Scale bars 1 mm.

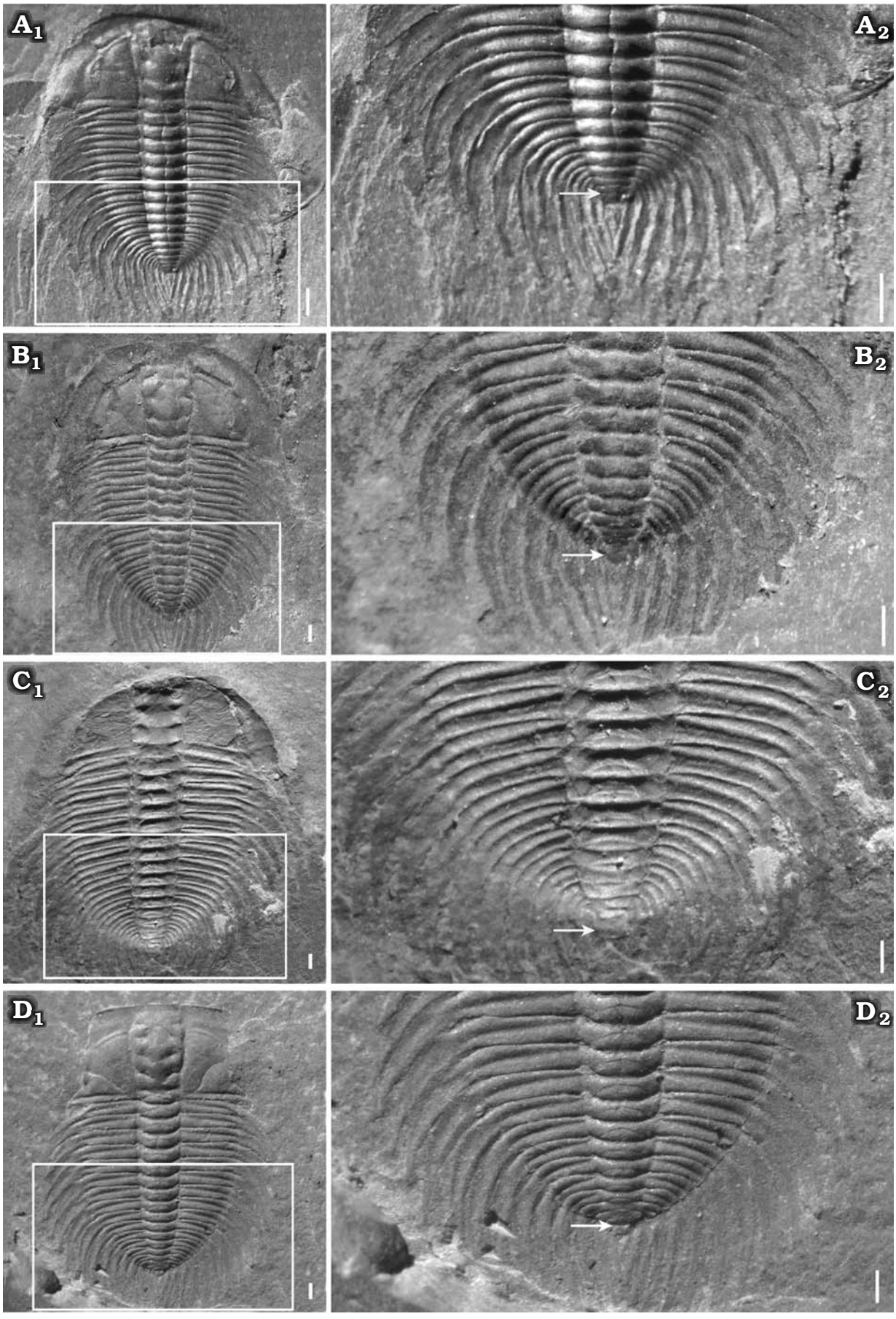
A1
A2
B1
B2
C1
C2
D1
D2

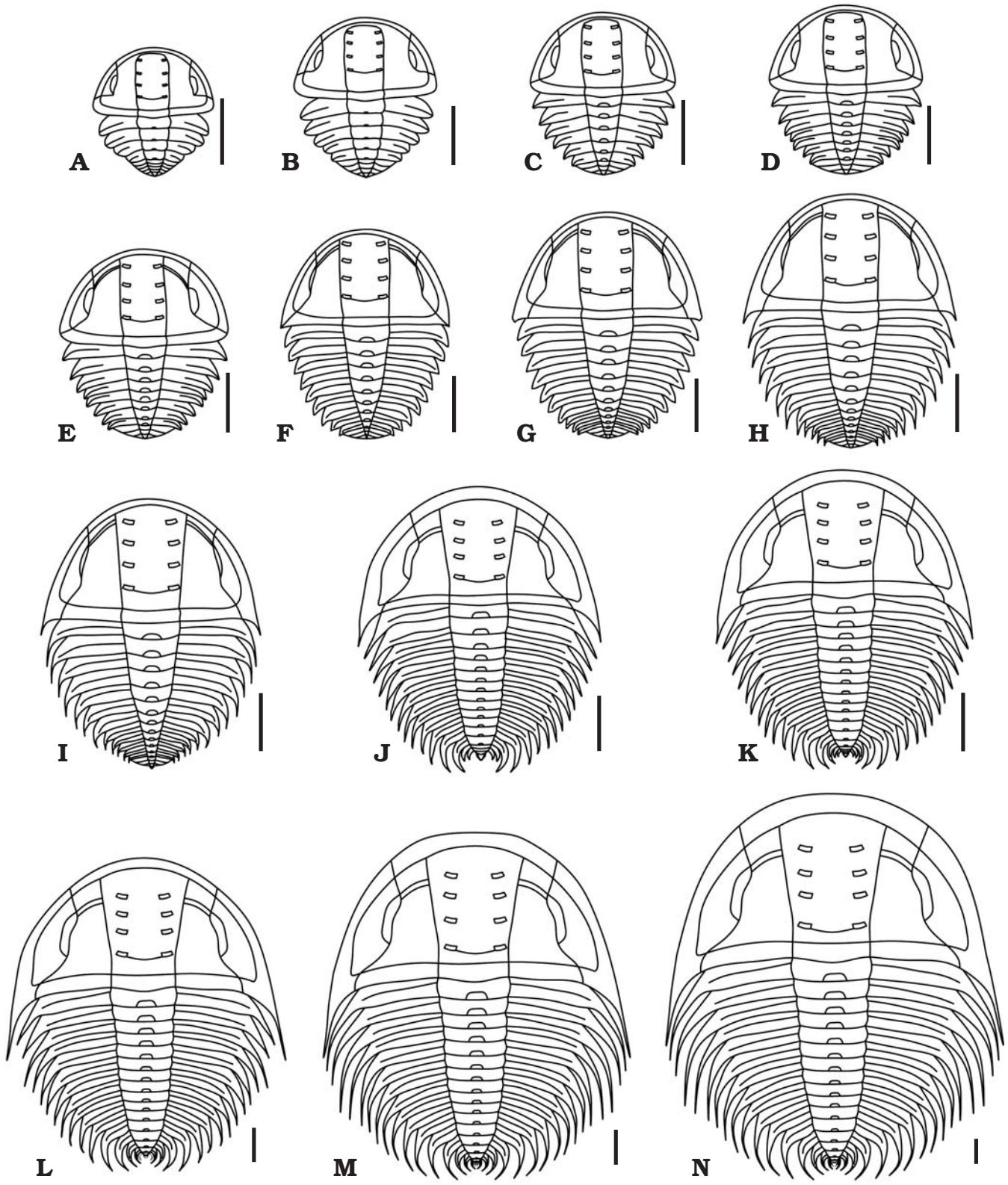

Fig. 7. Reconstructions in dorsal view of ontogenetic series of *Changaspis elongata* Lee in Chien, 1961. **A**–**M**. D4–16. **N**. H. Scale bars 1 mm.

← Fig. 6. Meraspid and holaspid exoskeletons of oryctocephalid trilobite *Changaspis elongata* Lee in Chien, 1961 from the Balang Formation (Cambrian Stage 4), Jianhe County, Guizhou Province, South China. **A**. D16, JLZ-160-1214; close-up of the last 11 thoracic segments and pygidium (A_2). **B**. H, JLZ-160-296; close-up of the last 11 thoracic segments and pygidium (B_2). **C**. H, JLZ-175-158; close-up of the last 12 thoracic segments and pygidium (C_2). **D**. H, JLZ-160-2796; close-up of the last 12 thoracic segments and pygidium (D_2). The arrows represent the position of the thoracic-pygidial boundary. Abbreviations: PY, pygidium; TS6–17, thoracic segments 6–17. Scale bars 1 mm.

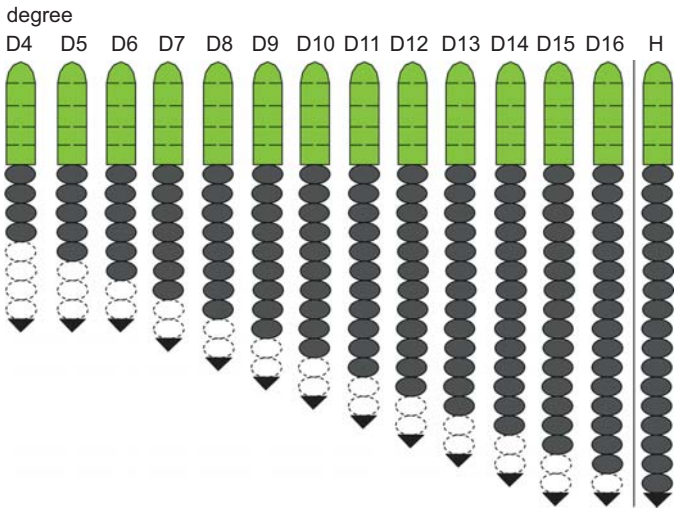

Fig. 8. Trunk development schedule of *Changaspis elongata* Lee in Chien, 1961. Green, dark grey, white, and black represent cephalon, thoracic segments, pygidial segments, and terminal axial piece, respectively. Dotted lines represent estimated, because of axial ring of pygidium faint.

(Table 2). Therefore, the growth rates of the thoracic segments are the same as that of the trunk.

From D10 to H the proportions of the 10th to 16th thoracic segments gradually increase, and the trend is gradually obvious (Fig. 9A) because the allometric coefficients with respect to trunk length are greater than 1 (Table 2). So, the growth rates of individual thoracic segments are faster than that of the trunk.

From D4 to H the posterior margin of each thoracic segment moves forward significantly with increasing thoracic segments (Fig. 9A) because the growth gradient exhibits increasing values from anterior (1st segment) to posterior (16th segment) (Fig. 10).

The proportion of the pygidium in the trunk gradually decreases (Fig. 9A) because the relative axial growth rate (+ standard error of the mean) of the pygidium (allometric coefficient with respect to the trunk length) is 0.31 + 0.0224. Therefore, the growth of pygidial length is slower than that of trunk length.

Table 2. Allometric coefficients and standard errors of the length of each thoracic segment relative to the trunk during the meraspid degrees 4–16 of *Changaspis elongata.*

Thoracic segments	Allometric coefficient	Standard error
1	0.71	0.02
2	0.70	0.02
3	0.76	0.03
4	0.76	0.03
5	0.84	0.02
6	0.87	0.02
7	0.89	0.04
8	0.99	0.02
9	1.00	0.03
10	1.06	0.03
11	1.1	0.03
12	1.16	0.04
13	1.15	0.09
14	1.16	0.17
15	1.18	0.18
16	1.23	0

Variations in the relative axial length of different body parts.—To further visualize the changes in the relative axial length of the cephalon, individual thoracic segments and pygidium, the quantitative studies of developmental traits were performed. The main changes (Fig. 9B) and reasons are as follows:

(i) During ontogeny, the ratio of the length of the cephalon to the body decreases gradually, while the ratio to the length of the trunk increases gradually (Fig. 9B). The various changes in the proportions of different body regions are mainly caused by the different AGR; that is, the average

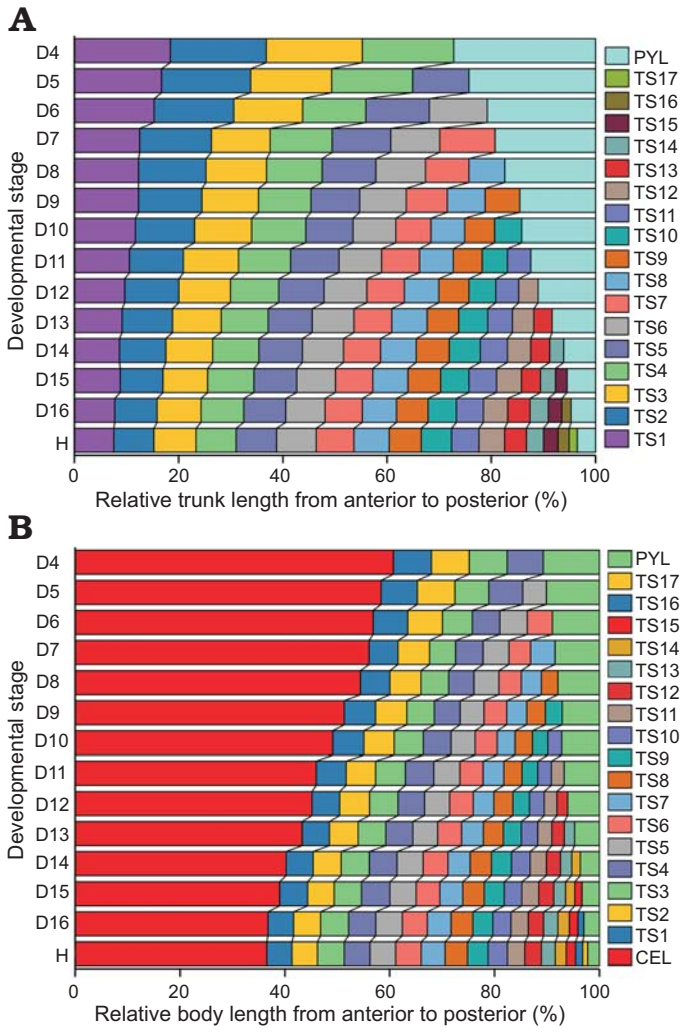

Fig. 9. Relative axial length of different body parts from the D4 to H stage of *Changaspis elongata* Lee in Chien, 1961. **A**. Relative trunk length of each thoracic segment and pygidium. **B**. Relative body length of cephalon, each thoracic segment and pygidium. Thorax and pygidium together constitute the trunk. Cephalon, thorax, and pygidium make up the body. Abbreviation: CEL, cephalic length; LTH, length of thorax; PYL, pygidial length; TS1, thoracic segment 1.

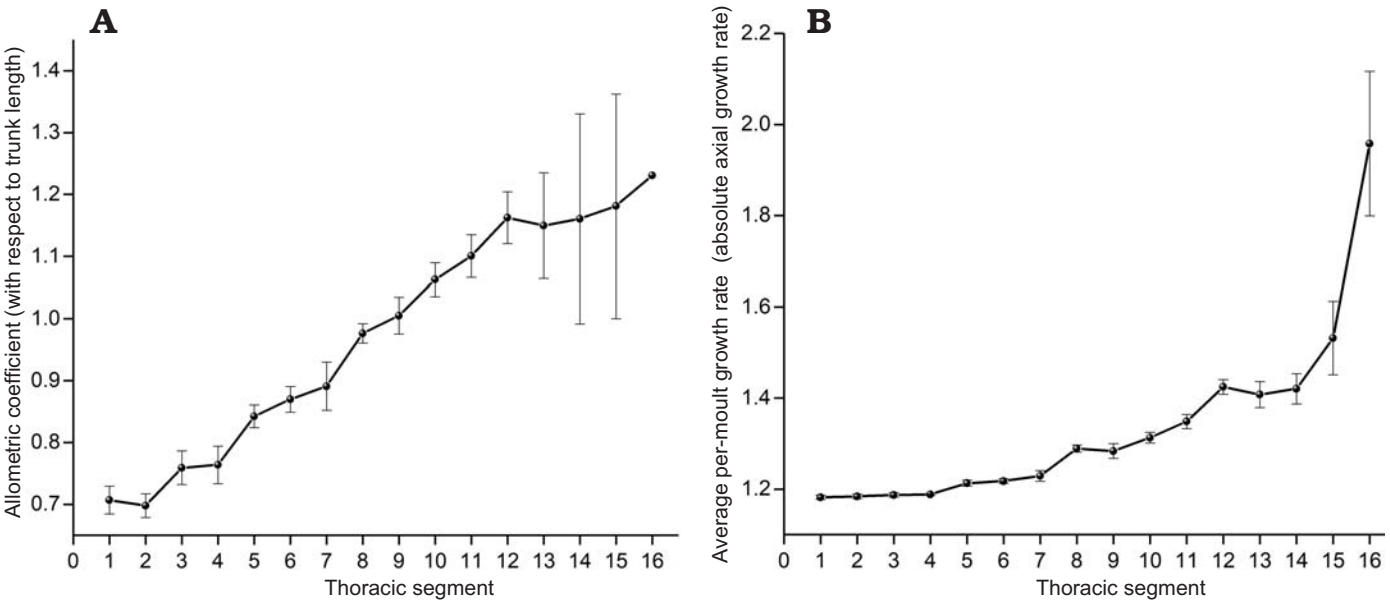

Fig. 10. Growth gradient in the trunk of *Changaspis elongata* Lee in Chien, 1961. **A**. Allometric coefficients of individual thoracic segments with respect to trunk length. **B**. Average per-moult growth rates of individual thoracic segments. Both exhibit significant increasing value from anterior to posterior (Spearman's rank correlation test, n = 16, $p_A = 0.988$, $p_B = 0.988$). Bars are standard errors caused by structural deformation and measurement (not calculable for TS16), n = 14 for TS1–4 and decreases from n = 13 to 2 for TS5–16, respectively. Abbreviation: TS1, section 1 thoracic segment.

growth rate of cephalic length is significantly lower than that of body length. However, the growth rate of the length of the trunk is significantly higher than that of body length (see below for AGR of different body parts).

(ii) With increasing thoracic segments, the relative position of the posterior margin of each segment moves forward gradually (Fig. 9B) because of the gradient, which results in higher growth rates of the thoracic segments from anterior to posterior (Fig. 10).

Growth gradient for relative axial growth rates.—The growth gradient is a distribution of the difference in growth rate along the body axis (Huxley 1994). In trilobites, a growth gradient has been used to analyse the different growth rates along the trunk axis of each segment (Fusco et al. 2014). The growth gradient for relative axial growth rates of each thoracic segment (allometric coefficients with respect to the trunk length, see Table 2) provides an intuitive indication of ontogenetic growth increments with respect to the trunk length. The growth gradient (Fig. 10A) reveals the following information:

(i) The allometric coefficients are 0.71–0.89, corresponding to the 1st to 7th thoracic segments, which is manifested as negative allometry (the allometric coefficients <1). The growth rates of each thoracic segment relative to the trunk length show slow growth.

(ii) The allometric coefficients corresponding to the 8th and 9th thoracic segments are 0.99–1.00, presenting isometry (the allometric coefficients ≈1). The growth rates of each thoracic segment are uniform with respect to the trunk length.

(iii) The allometric coefficients corresponding to the 10th to 16th thoracic segments are 1.06–1.23, showing positive allometry (the allometric coefficients >1). The growth rates of each thoracic segment relative to the trunk length show fast growth.

(iv) The relative axial growth rates exhibit obviously increasing values from anterior to posterior. The numbers of thoracic segments with positive and negative allometry account for exactly half of the total number of thoracic segments.

(v) The growth gradient (Fig. 10A) visually explains the variation in the ratio of each thoracic segment to trunk length from D4 to H (Fig. 9A).

Growth gradients for absolute axial growth rates.—Morphometric analysis shows the growth gradient (Fig. 10B) for AGR (absolute axial growth rates) of each thoracic segment from D4 to H. Although the growth gradient of per-moult growth rates shows a slower growth trend from anterior to posterior than the relative axial growth rates, the growth gradient also shows a gradual growth trend from anterior to posterior. The growth gradients of increasing values from anterior to posterior illustrate that the reason why the growth gradient for relative axial growth rates (Fig. 10A) exhibits an increasing trend from anterior to posterior is that the absolute axial growth rates of the newly increased segments increase gradually with increasing thoracic segments from D4 to H.

Average per-moult growth rates of the different body parts.—The values of AGR provide a more intuitive indication of individual growth increments beyond descriptive ontogenetic studies. By implementing morphometric analysis, the AGR (+ standard error of the mean) for the lengths of the body, cephalon and trunk are 1.19 + 0.00862, 1.15 + 0.00761, and 1.24 + 0.0095, respectively. The cephalic length has an AGR (+ standard error of the mean) that is lower than that

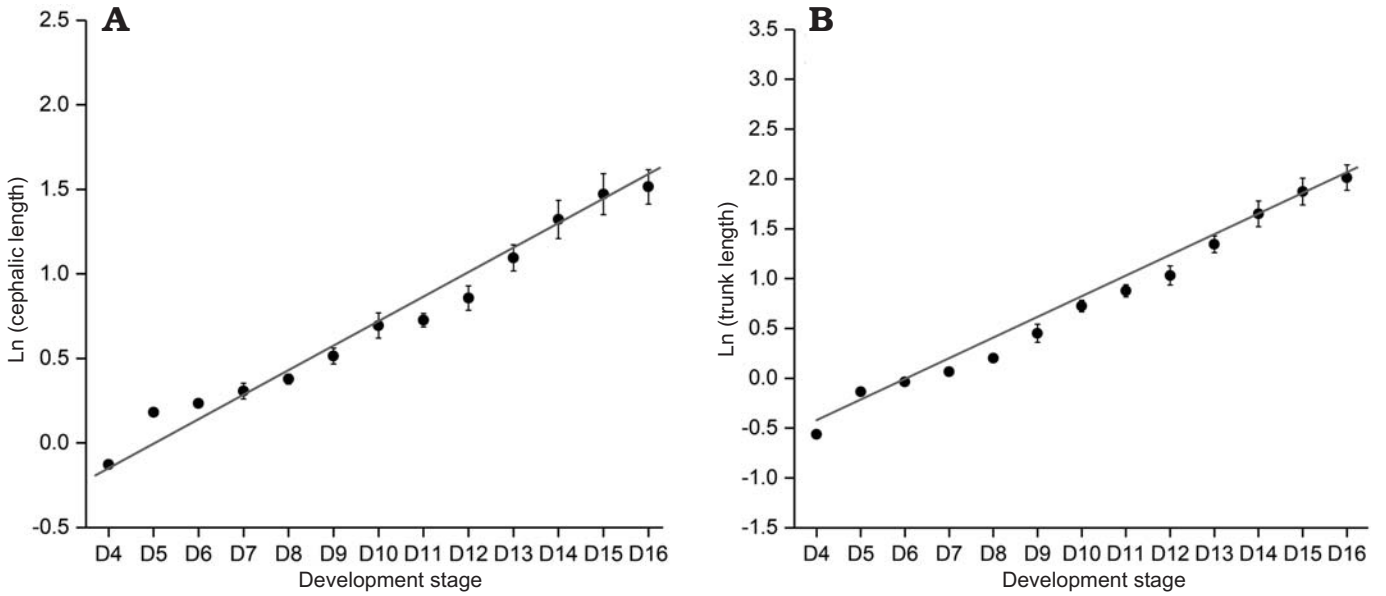

Fig. 11. Ontogenetic size progression from D4 to D16 of *Changaspis elongata* Lee in Chien, 1961. **A**. Least square linear regression of ln CEL_d on the d stage ($r_A = 0.96622$, n = 13). **B**. Least square linear regression of ln TRL_d on the d stage ($r_B = 0.98373$, n = 13). Bars are mean standard errors caused by structural deformation and measurement. Abbreviation: CEL_d, cephalic length on the d stage; TRL_d, trunk length on the d stage.

of the body length, 1.15 + 0.00761 versus 1.19 + 0.00862 (one-tailed Student's t-test, p = 5.11549E-06) in D4–16. However, the length of the trunk has an AGR (+ standard error of the mean) that is higher than that of the body length, 1.24 + 0.0095 versus 1.19 + 0.00862 (one-tailed Student's t-test, p = 1.59036E-05). Therefore, the different values of the average growth rates indicate different changes between the cephalon and trunk in proportions along the axial length of the body (Fig. 9B).

Growth progression and Dyar's rule.—Among the rules describing the increment of discrete size, the Dyar rule (Dyar 1890) is considered a null model of arthropod growth (Klingenberg and Zimmermann 1992; Fusco et al. 2004). From meraspid degree 4 to the holaspid period, we make a scatter plot of the natural logarithm of the lengths of cephalon and trunk during the meraspid period and then perform least square linear regressions on the dataset (Fig. 11). The high values of the coefficients of determination of the regressions ($r^2_A = 0.97496$, $r^2_B = 0.98752$, n = 13; r^2_A and r^2_B represent goodness of fit) suggest that the growth progression of the lengths of the cephalon and trunk conform to a progression at a constant rate (Dyar's rule).

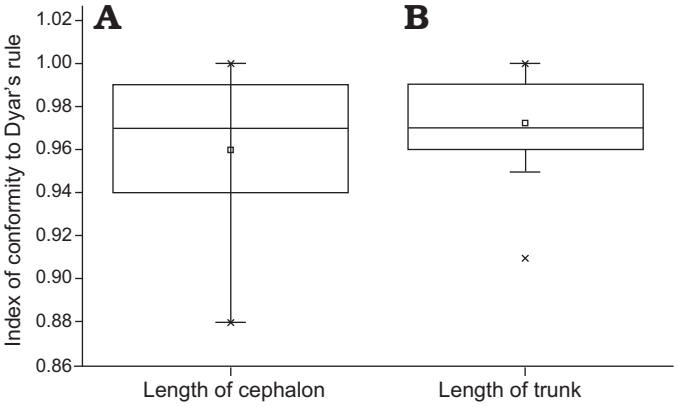

Fig. 12. Boxplot showing the relationship about the index of conformity to Dyar's rule for the cephalic and trunk length of *Changaspis elongata* Lee in Chien, 1961. The middle line in the box, which is the median of the dataset, represents the average of the sample data. The width of the box partly reflects the volatility of the dataset. Above and below the box, there is a line, respectively represent the maximum and minimum value.

By adopting a "coarse-grained" quantitative approach, we further assess the IDC (Fusco et al. 2012). The variation range of IDC for the cephalic length is 0.88–1.00, and the median value is 0.97; the variation range of IDC for the trunk length is 0.91–1.00, and the median value is 0.97. Figure 12 shows that the average level (the median) of the IDC for the cephalon is equal to that of the trunk; however, the fluctuation range of IDC for the cephalon is larger than that for the trunk.

In meraspids, although the distribution of IDC for trunk length is significantly different from that of cephalic length (Wilcoxon test on medians between cephalic length and trunk length, P = 0.02453, Fig. 13), the distribution of IDC of the values for the lengths of the cephalon and trunk are greater than 0.85. Therefore, the distribution of IDC of the values shows that the growth progressions of the lengths of the cephalon and trunk both conform to Dyar's rule during the meraspid period degrees 4–16.

Discussion

As for corynexochide trilobites from the early Cambrian, the trunk segmentation sequence of trilobites has been widely discussed (e.g., Hou et al. 2015; Dai et al. 2014, 2017; Du et al. 2018). The development models of *Arthricocephalus*

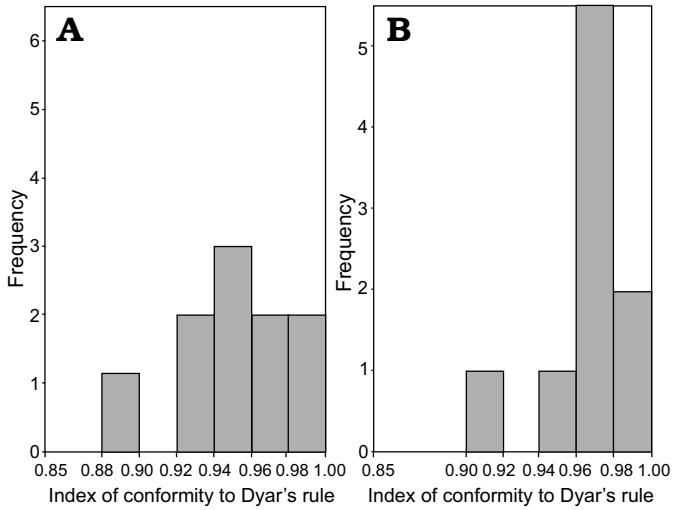

Fig. 13. Frequency distribution of the index of conformity to Dyar's rule from the D4 to D16 of *Changaspis elongata* Lee in Chien, 1961. **A**. Cephalic length (n = 13). **B**. Trunk length (n = 13).

chauveaui, *C. elongata*, and *Duodingia duodingensis* show hypoprotomeric development; that is, the trunk segmentation sequences suggest that the epimorphic phase begins within the meraspid phase (Hughes et al. 2006). Hou et al. (2015) discussed intraspecific polymorphism of *Hunanocephalus ovalis* in the pattern of segment release; and the trunk segmentation sequences in this species show that the onset of epimorphosis precedes or occurs synchronously at the onset of the holaspid phase. Therefore, the development models of *H. ovalis* can be divided into hypoprotomeric and synarthromeric developments (Hughes et al. 2006). In addition, the trunk segmentation sequence of *Duyunnaspis duyunensis* shows that the onset of the holaspid phase precedes the onset of the epimorphic phase (Dai et al. 2017). Therefore, the development model of *D. duyunensis* belongs to protarthrous development (Hughes et al. 2006). By comparing the trunk segmentation sequences of these trilobites, we find that the developmental modes of the corynexochida trilobites from the early Cambrian show different developmental modes. This phenomenon may suggest that diverse developmental modes represent the ancestral mode of euarthropod development.

Dyar's rule has proved to be a good model for post-embryonic development of many extant arthropods (Klingenberg and Zimmermann 1992) and trilobites (Chatterton and Speyer 1997; Fusco et al. 2004, 2012). It has been reported that the different characters and portions of the ontogeny of various trilobites are highly consistent with Dyar's rule (Chatterton and Speyer 1997; Fusco et al. 2012). The length of trunk and cephalon of *Changaspis elongata* are also highly consistent with Dyar's rule. This implies that the different traits of the ontogeny of early Cambrian trilobites may be highly consistent with Dyar's rule.

Silurian trilobite *Aulacopleura koninckii* is one of the most thoroughly studied trilobite species (Fusco et al. 2004, 2014, 2016; Hughes et al. 2017). Our results show that the thoracic axial growth gradient of *C. elongata* exhibits a significant decreasing AGR values from posterior to anterior. Although the AGR values for each thoracic segment of *C. elongata* and *A. koninckii* are different, the thoracic axial growth gradients of *C. elongata* and *A. koninckii* are generally quite similar, indicating that the growth rates decrease from posterior to anterior in the thorax during ontogeny. More importantly, this result suggests that the segment growth dynamics in the thorax of trilobites from early Cambrian to Silurian followed the same general continuous, steady-state growth gradient decreasing from posterior to anterior.

In addition, the AGR (+ standard error of the mean) for the meraspid cephalic and trunk lengths in *A. koninckii* are 1.087±0.004 and 1.115±0.003, respectively (Fusco et al. 2014, 2016). The AGR (+ standard error of the mean) for the meraspid cephalic and trunk lengths in *C. elongata* are 1.147±0.007 and 1.24±0.01, respectively. The AGR for the meraspid trunk length are higher than those for the cephalic length. This result is expected because the growth of the trunk is commonly more complex than that of the cephalon. The complexity relates to the fact that premature thoracic and pygidial growth includes not only the growth of individual segments but also dynamic changes in the number of the segments.

Fusco et al. (2014) revealed an increasing trend in growth gradients from anterior to posterior in the trunk of *A. koninckii* for absolute axial growth rates and relative axial growth rates. Morphological analysis and function fitting test analyses support segment growth depending on the position of a formal specification along the trunk main axis, governed by a continuous, stable growth gradient (Fusco et al. 2014). After examining the previous research results of reconstructing the post-embryonic ontogeny of *A. koninckii*, the post-embryonic ontogeny is reconstructed by applying inferred development parameters related to size, shape and segmentation (Hughes et al. 2017). Although this paper does not test two alternative hypotheses of growth control associated with the gradient, including segment-specific control and regional control (Fusco et al. 2014), the variations in the relative axial length of different body parts (Fig. 9B) reveal that the posterior margin of individual thoracic segments moves forward significantly with the increase in thoracic segments, consistent with a previous study on relative axial length of different body parts of *A. koninckii* during the meraspid period (Hughes et al. 2017). Hence, we speculate that the segmental growth control of *C. elongata* may depend on the form of the specification along the position of the trunk main axis, controlled by a continuous, stable growth gradient. An expanded trilobite ontogenesis database is expected to provide important additional insights into how the developmental traits of an ancient, diverse and rapidly radiating arthropod branch evolved (Fusco et al. 2012). In addition, a reliable assessment of the palaeo-evo-devo approach to arthropod evolution will require the extension of quantitative study for developmental traits of *A. koninckii* to a variety of

other trilobites, of which the studies for trilobites from the early Cambrian are likely be fruitful (Hughes et al. 2017). Therefore, the developmental traits and the new dataset in this paper are important and representative. On the one hand, they provide an important basis for further quantitative detection of the segment growth dynamics of growth control for the development of trunk in the future. On the other hand, early Cambrian trilobites are phylogenetically basal within the clade, so it is possible to gain a deep understanding by investigating the primitive development traits of early Cambrian trilobites (Hughes et al. 2017).

Conclusions

A relatively continuous ontogenetic sequence reveals that the holaspides of *Changaspis elongata* have seventeen thoracic segments and that the number of pygidial segments gradually decreases from meraspid degree 4 to the holaspid period. This demonstrates that the corynexochida trilobites from the early Cambrian show various models for trunk development. By implementing morphometric analysis of the data, this study reveals that after segment addition is completed, Dyar's rule is proved to be a good model for post-embryonic development of *C. elongata*. The reconstruction of the development of *C. elongata* allows visualization of the changes in relative growth and segmentation for the different body parts. The growth gradients and the average growth rates of the body, cephalon and trunk explain different variations in the relative axial lengths of different body parts. Our results show that the segment growth dynamics in the thorax of early Cambrian to Silurian trilobites follow the same general continuous, steady-state growth gradient decreasing from posterior to anterior.

Acknowledgements

We thank Tae-Yoon S. Park (Korea Polar Research Institute(Seoul, Korea), Frederick Sundberg (Show Low, Arizona, USA) and two anonymous reviewers for their thoughtful review and helpful suggestions, which improved this manuscript. Special thanks to Nigel C. Hughes (University of California, Riverside, USA) for encouraging me to study the ontogeny of trilobites and providing many useful comments on my manuscript. We would like to express sincere thanks to Giuseppe Fusco (University of Padova, Italy) for kind assistance to this paper of calculation method of the growth gradients and useful suggestions. Thanks to Shuai Liu (Guizhou University, China), Rong-Qin Wen (Guizhou University, China) and Yu-Juan Liu (Guizhou University, China) for their assistance in fieldwork. Thanks to Tian Lan (Guizhou University, China) for linguistic improvements on my manuscript. This research is supported by the National Sciences Foundation of China (Grant No. 40672005), the Guizhou Science and Technology Department, China (Grant No. Gui, Sci. Z.[2014]4003; Gui Sci G[2017] 5788), and the Strategic Priority Research Program of Chinese Academy of Sciences, Grant No. XDB2600000.

References

Barrande, J. 1852. *Système silurien du centre de la Bohême. I: Recherches paleontologiques*. 935 pp. Published by the author, Praha.

Bergeron, J.N. 1899. Etude de quelques trilobites de Chine. *Bulletin de la Société Géologie France* 27: 499–516.

Chien, Y.Y. 1961. Cambrian trilobites from Sandu and Du yun, southern Kweichou [in Chinese, with English summary]. *Acta Palaeontologica Sinica* 9: 91–129.

Chatterton, B.D.E. and Speyer, S.E. 1997. Ontogeny. *In*: R.L. Kaesler (ed.), *Treatise on Invertebrate Paleontology, Part O, (Arthropoda 1, revised)*, 173–247. Geological Society of America and University of Kansas Press, Boulder, Colorado and Lawrence, Kansas.

Dyar, H.G. 1890. The number of molts of lepidopterous larvae. *Psyche* 5: 420–422.

Dai, T., Zhang, X.L., and Peng, S.C. 2014. Morphology and ontogeny of *Hunanocephalus ovalis* (trilobite) from the Cambrian of South China. *Gondwana Research* 25: 991–998.

Dai, T., Zhang, X.L., Peng, S.C., and Yao, X.Y. 2017. Intraspecific variation of trunk segmentation in the oryctocephalid trilobite *Duyunaspis duyunensis* from the Cambrian (Stage 4, Series 2) of South China. *Lethaia* 50: 527–539.

Du, G.Y., Peng, J., Wang, D.Z., Wen, R.Q., and Liu, S. 2018. Morphology and trunk development of the trilobite *Arthricocephalus chauveaui* from the Cambrian series 2 of Guizhou, South China. *Historical Biology* [published online, https://doi.org/10.1080/08912963.2018.1476857]

Esteve, J., Zhao, Y.L., and Peng, J. 2017. Morphological assessment of the Cambrian trilobites *Oryctocephalus indicus* (Reed 1910) from China and *Oryctocephalus* "*reticulatus*" (Lermontova 1940) from Siberia. *Lethaia* 50: 175–193.

Fusco, G., Garland, T. Jr., Hunt, G., and Hughes, N.C. 2012. Developmental trait evolution in trilobites. *Evolution* 66: 314–329.

Fusco, G., Hong, P. S., and Hughes, N.C. 2014. Positional specification in the segmental growth pattern of an early arthropod. *Proceedings of the Royal Society B: Biological Sciences* 281: 20133037.

Fusco, G., Hong, P.S., and Hughes, N.C. 2016. Axial growth gradients across the post-protaspid ontogeny of the Silurian trilobite *Aulacopleura koninckii*. *Paleobiology* 42: 426–438.

Fusco, G., Hughes, N.C., Webster, M., and Minelli, A. 2004. Exploring developmental modes in a fossil arthropod: growth and trunk segmentation of the trilobite *Aulacopleura koninckii*. *American Naturalist* 163: 167–183.

Huxley, J.S. 1994. Problems of relative growth. *Journal of Anatomy* 50: 893.

Hughes, N.C., Hong, P.S., Hou, J.B., and Fusco, G. 2017. Trilobite *Aulacopleura koninckii* reconstructed by applying inferred growth and segmentation dynamics: a case study in Paleo-Evo-Devo. *Frontiers in Ecology and Evolution* 5: 1–12.

Hughes, N.C., Minelli, A., and Fusco, G. 2006. The ontogeny of trilobite segmentation: a comparative approach. *Paleobiology* 32: 602–627.

Hou, J.B., Hughes, N.C., Lan, T., Yang, J., and Zhang, X.G. 2015. Early postembryonic to mature ontogeny of the oryctocephalid trilobite *Duodingia duodingensis* from the lower Cambrian (Series 2) of southern China. *Papers in Palaeontology* 1: 497–513.

Klingenberg, C.P., and Zimmermann, M. 1992. Dyar's rule and multivariate allometric growth in nine species of waterstriders (Heteroptera: Gerridae). *Journal of Zoology* 227: 453–464.

Lu, Y.H., Qian, Y.Y., and Zhu, Z.L. 1963. *Trilobita* [in Chinese]. 186 pp. Science Press, Beijing.

Lei, Q.P. 2015. New ontogenetic information on *Duyunaspis duyunensis* Zhang & Qian in Zhou et al., 1977 (Trilobita, Corynexochida) from the Cambrian and its possible sexual dimorphism. *Alcheringa: An Australasian Journal of Palaeontology* 40: 12–23.

Liang, B.Y., Peng, J., and Wen, R.Q. 2017. Ontogeny of the trilobite *Redlichia (Pteroredlichia) chinensis* (Walcott. 1905) from the Cambrian Balang Formation [in Chinese, with English summary]. *Acta Palaeontologica Sinica* 56: 25–36.

Lu, Y.H., Zhu, Z.L., Qian, Y.Y., Lin, H.L., Zhou, Z.Y., and Yuan, K.X.

1974. Bio-environmental control hypothesis and its application to Cambrian biostratigraphy and palaeozoogeography [in Chinese, with English summary]. *Memoir of the Nanjing Institute of Geology and Palaeontology, Academia Sinica* 5: 27–110.

McNamara, K.J., Yu, F., and Zhou, Z.Y. 2003. Ontogeny and heterochrony in the oryctocephalid trilobite *Arthricocephalus* from the Early Cambrian of China. *Special Papers in Palaeontology* 70: 103–126.

McNamara, K.J., Yu, F., and Zhou, Z.Y. 2006. Ontogeny and heterochrony in the Early Cambrian oryctocephalid trilobites *Changasips*, *Duyunaspis* and *Balangia* from China. *Palaeontology* 49: 1–19.

Peng, J., Zhao, Y.L., and Yang, X.L. 2006. Trilobites of the upper part of lower Cambrian Balang Formation, southeastern Guizhou Province, China [in Chinese, with English summary]. *Acta Palaeontologica Sinica* 45: 235–242.

Peng, J., Zhao, Y.L., Wu, Y., Yuan, J.L., and Tai, T. 2005. The Balang Fauna —a new early Cambrian Fauna from Kaili City, Guizhou Province. *Chinese Science Bulletin* 50: 1159–1162.

Qin, Q., Peng, J., Fu, X., and Da, Y. 2010. Restudy of Changaspis (Lee), 1961 from Qiandongian (Early Cambrian) Balang Formation near eastern Guizhou, south China [in Chinese, with English summary]. *Acta Palaeontologica Sinica* 49: 220–230.

Reed, F.R.C. 1910. The Cambrian fossils of Spiti. *Palaeontologia Indica Series* 15: 1–70.

Shen, Z., Peng, J., Wen, R.Q., and Liu, S. 2016. *Arthricocephalites* (trilobite) from the Cambrian and its stratigraphic significance [in Chinese, with English summary]. *Acta Palaeontologica Sinica* 55: 9–18.

Walcott, C.D. 1905. Cambrian faunas of China. *Proceedings of the United States National Museum* 29: 1–106.

Yuan, J.L., Zhao, Y.L., Wang, Z.Z., Zhou, Z., and Chen, X.Y. 1997. A preliminary study on Lower–Middle Cambrian boundary and trilobite fauna at Balang, Taijiang, Guizhou, South China [in Chinese, with English summary]. *Acta Palaeontologica Sinica* 36: 494–524.

Zhou, T.M., Liu, Y.R., Meng, X.S., and Sun, Z.H. 1977. Trilobita [in Chinese, with English summary]. *In*: Geological Bureau of Henan Province (ed.), *Palaeontological Atlas of Central and South China. Guizhou 1*, 107–266. Geological Publishing House, Beijing.